Wigner Crystallization in Mesoscopic 2D Electron Systems

A. V. Filinov,[1,2] M. Bonitz,[1] and Yu. E. Lozovik[2]
[1]*Fachbereich Physik, Universität Rostock Universitätsplatz 3, D-18051 Rostock, Germany*
[2]*Institute of Spectroscopy, 142090 Troitsk, Moscow Region, Russia*
(Received 25 April 2000)

Wigner crystallization of electrons in 2D quantum dots is reported. It proceeds in two stages: (i) via radial ordering of electrons on shells and (ii) freezing of the intershell rotation. The phase boundary of the crystal is computed in the whole temperature-density plane, and the influences of quantum effects and the particle number are analyzed.

DOI: 10.1103/PhysRevLett.86.3851 PACS numbers: 73.21.–b, 73.22.–f

In recent years there is growing interest in *finite quantum* systems at high density and/or low temperature. In particular, the behavior of a small number of electrons in quantum dots is actively investigated both experimentally [1] and theoretically [2,3]. The limiting behavior of two-dimensional (2D) finite quantum systems at *zero temperature* has been studied by unrestricted Hartree-Fock calculations [2] which revealed a transition from a Fermi liquid to an ordered state called "Wigner molecule." The same crossover at *finite temperature* has been recently demonstrated by fermionic path integral Monte Carlo simulations [3]. It has to be expected that further increase of correlations (increase of the Brueckner parameter r_s) will lead to a still higher ordered quantum state resembling the Wigner crystal (WC) [4,5].

On the other hand, for *finite classical systems,* Monte Carlo simulations have shown evidence of crystallization for sufficiently large values of the coupling parameter $\Gamma = U/k_BT$, where U is the interaction energy. These classical clusters consist of well-separated shells [6–9], and melting proceeds in two stages: first, orientational disordering of shells takes place—neighboring shells may rotate relative to each other while retaining their internal order. Further growth of thermal fluctuations leads to shell broadening and overlap—radial melting. The temperature of radial melting T_r may be many orders of magnitude higher than the orientational melting temperature T_o [8]. Large clusters with $N > 100$ have a regular triangular lattice structure and exhibit only radial melting.

Now the question arises, how does the behavior of finite electron clusters change at low temperature, i.e., in the *quantum regime*? In this Letter we demonstrate that, indeed, Wigner crystallization in 2D quantum electron clusters exists and that it is accompanied by two distinct—radial and orientational—ordering transitions too. However, in contrast to classical clusters, we observe a new melting scenario which is caused by quantum fluctuations and exists even at zero temperature ("cold" melting [10]). We present a detailed analysis of the two-stage quantum melting process and provide numerical data for the phase boundaries of both crystal phases, for particle numbers in the range $N = 10–20$.

Model and characteristic parameters.—The theoretical analysis of quantum confined electrons at finite temperature requires the simultaneous account of strong correlations and quantum effects which excludes, e.g., perturbation or mean field methods. We, therefore, use a path integral Monte Carlo (PIMC) approach. We consider a finite unpolarized [11] 2D system of N electrons at temperature T. The electrons interact via the repulsive Coulomb potential and are confined in a harmonic trap of strength ω_0. The system is described by the Hamiltonian

$$\hat{H} = \sum_{i=1}^{N} \frac{\hbar^2 \nabla_i^2}{2m_i^*} + \sum_{i=1}^{N} \frac{m_i^* \omega_0^2 r_i^2}{2} + \sum_{i<j}^{N} \frac{e^2}{\epsilon_b |\mathbf{r}_i - \mathbf{r}_j|}, \quad (1)$$

where m^* and ϵ_b are the effective electron mass and background dielectric constant, respectively. We use the following length and energy scales: r_0, given by $e^2/\epsilon_b r_0 = m^* \omega^2 r_0^2/2$, and E_c, the average Coulomb energy, $E_c = e^2/\epsilon_b r_0$. After the scaling transformations $\{r \to r/r_0, E \to E/E_c\}$ the Hamiltonian takes the form

$$\hat{H} = \frac{n^2}{2} \sum_{i=1}^{N} \nabla_i^2 + \sum_{i=1}^{N} r_i^2 + \sum_{i<j}^{N} \frac{1}{|\mathbf{r}_i - \mathbf{r}_j|}, \quad (2)$$

where $n \equiv \sqrt{2}\, l_0^2/r_0^2 = (a_B^*/r_0)^{1/2}$, a_B^* is the effective Bohr radius, and $l_0^2 = \hbar/(m^*\omega_0)$ is the extension of the ground state wave function of noninteracting trapped electrons. Further, we define, in analogy to macroscopic systems, $r_s \equiv r_0/a_B^* = 1/n^2$ [12]. (Note that in mesoscopic clusters, r_s and n characterize only the average electron density.) Finally, we introduce the dimensionless temperature $T \equiv k_BT/E_c$ which allows us to define $\Gamma \equiv 1/T$ [7,12].

To obtain the configuration and thermodynamic properties of clusters of N electrons described by the Hamiltonian (2), we performed fermionic PIMC simulations using a standard bisection algorithm [13]. The number of time slices M has been varied with n and T according to $M = ln/T$, where l was typically in the range of 1–10 to achieve an accuracy better than 5% for the quantities (3) and (4); see below. To obtain the phase boundary of the Wigner crystal, calculations in a broad range of parameter values

$\{n, T, N\}$ were performed. For each set of parameters, several independent Monte Carlo runs consisting of approximately 10^6 steps were carried out.

Structure of electron clusters.—The simulations yield the spatial electron configurations in the trap [14], examples of which are shown in Figs. 1 and 2. One clearly sees the formation of shells. Our analysis revealed the same shell structures as reported for the corresponding classical systems [6,7]. The number of shells and shell occupation depend on N; cf. Table I. Clusters, in which the particle number on the outer shells are multiples of those on the inner shells, have the highest symmetry which leads to particular properties. Examples of these *magic numbers* are $N = 10, 12, 16, 19$; cf. Table I. Let us now discuss the influence of quantum effects on the clusters. In contrast to classical systems, where the electrons are pointlike particles, in our case, the wave function of each electron has a finite width and may be highly anisotropic, which is typical for low temperature, as is most clearly seen in Fig. 1(a). This peculiar shape results from a superposition of N-body correlations, quantum effects, and the confinement potential. Varying the density and temperature, the shape changes in a very broad range, which can lead to qualitative transitions of the cluster, including cold quantum melting, as will be shown below.

Melting and phase transitions.—Wigner crystallization is known to occur when the ratio of the Coulomb energy to the kinetic energy exceeds a certain threshold. In the quantum and classical limits, this ratio is given by the Brueckner parameter r_s and the classical coupling parameter Γ, respectively. Let us first consider the *classical case*. At sufficiently low T (high Γ), a classical cluster is in the orientationally and radially ordered crystal phase. Our simulations revealed that in a finite system (in the classical part of the phase space), both orientational and radial melting are determined by characteristic values of Γ which, however, strongly depend on the particle number N. We find that orientational melting occurs at temperatures which vary over many orders of magnitude, $T_o^* \approx 3 \times 10^{-3}$–$10^{-12}$ and are very sensitive to the shell configuration, as observed in Ref. [8]. Higher temperatures (lower Γ) are found for *magic* clusters; cf. Table I. The magic cluster with $N = 19$ has unusual stability against intershell rotation, as the ratio of particle numbers on the three shells is optimal for the formation of a triangular lattice. In contrast, nonmagic clusters have much lower orientational melting temperatures (see Table I), which is particularly striking for $N = 20$. The situation is completely different at radial melting. Here, the critical temperatures for intershell particle jumps (radial disordering) for magic clusters have been found to be approximately 2 times smaller than those for nonmagic clusters (Table I).

We now investigate the phenomenon of *quantum orientational melting* (OM). As an illustration, consider the cluster with $N = 12$ particles. Figure 1 shows three snapshots of particle configurations at low temperature where the density increases from (a) to (c), and (b) corresponds to the critical density. One of the characteristic features of quantum OM is a high anisotropy of the electron wave function. Its main spread is along a high and narrow ravine formed by the many-body potential. The growth of quantum fluctuations from 1(a) to 1(c) is predominantly in

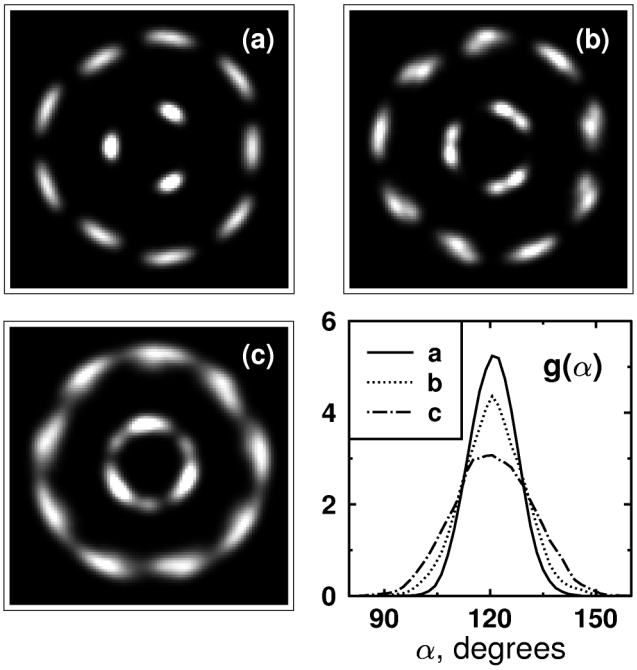

FIG. 1. Snapshots of the cluster with 12 electrons [14], (a) in the orientationally ordered state ($n = 0.01$); (b) at orientational melting ($n = 0.014$); (c) in the orientationally disordered/radially ordered state ($n = 0.02$). Lower right figure shows the corresponding angular pair distribution functions for electrons on the inner shell. $T = 1.0 \times 10^{-4}$.

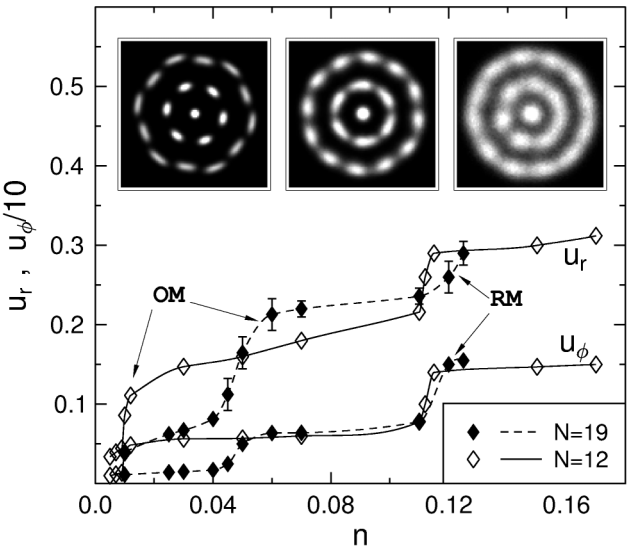

FIG. 2. Relative angular and radial fluctuations, Eqs. (3) and (4), in the vicinity of orientational (OM) and radial melting (RM) for $N = 12$ and $N = 19$ versus density. Insets show snapshots of the "magic" cluster with $N = 19$ in the three phases (left, $n = 0.025$; middle, $n = 0.06$; right, $n = 0.14$). $T = 5.0 \times 10^{-4}$. Error bars shown are typical for all curves.

TABLE I. *Classical* Wigner crystal: critical temperature T^* and coupling parameter Γ^* corresponding to the orientational (o) and radial (r) melting for clusters of size N in the classical limit ($n \to 0$). Second column contains the shell occupancy, starting from the inner shell. Nonmagic clusters are typed italic.

N		T_o^*	Γ_o^*	T_r^*	Γ_r^*
10	2, 8	1.5×10^{-5}	6.7×10^{4}	5.9×10^{-3}	169
11	*3, 8*	*2.6×10^{-7}*	*3.85×10^{6}*	*1.25×10^{-2}*	*80*
12	3, 9	8.0×10^{-4}	1250	6.0×10^{-3}	166
16	1, 5, 10	1.7×10^{-3}	590	6.2×10^{-3}	161
19	1, 6, 12	3.0×10^{-3}	330	6.5×10^{-3}	154
20	*1, 7, 12*	*2.9×10^{-12}*	*3.4×10^{11}*	*1.2×10^{-2}*	*83*

angular direction leaving the radial component practically unchanged. Figure 1(b) shows that, at quantum OM, the probability density of each inner shell electron splits in two maxima which are due to electron transitions between two closely lying energy levels. At still higher density, Fig. 1(c), the electron wave function spreads further, splitting into three maxima, and it starts to spread in a radial direction. Obviously, OM is accompanied by intensification of angular distance fluctuations; cf. Fig. 1(d). The spread of the electron wave functions smears out the energy barrier for intershell rotation which, in turn, reduces the melting temperature. In the limit $T \to 0$ this leads to so-called cold orientational melting.

To allocate the melting temperatures and densities accurately, we examine the relative mean angular distance fluctuations of particles from different shells

$$u_\phi \equiv \sqrt{\langle \delta\phi^2 \rangle} = \frac{2}{m_{s_1} m_{s_2}} \sum_i^{m_{s_1}} \sum_j^{m_{s_2}} \sqrt{\frac{\langle |\phi_j - \phi_i|^2 \rangle}{\langle |\phi_j - \phi_i| \rangle^2} - 1}\,, \tag{3}$$

where ϕ_i and ϕ_j are the angular positions of particles on shells s_1 and s_2, respectively, and m_{s_1} and m_{s_2} are the total number of particles on the shells. We further consider the magnitude of the relative distance fluctuations

$$u_r \equiv \sqrt{\langle \delta r^2 \rangle} = \frac{2}{N(N-1)} \sum_{i \le j}^{N} \sqrt{\frac{\langle r_{ij}^2 \rangle}{\langle r_{ij} \rangle^2} - 1}\,, \tag{4}$$

where r_{ij} is the distance between particles i and j. We found that, in the vicinity of orientational and radial melting, quantities (3) and (4) show a strong increase, thus providing a suitable quantitative criterion for these phase transitions, as can be seen in Fig. 2.

We computed the n dependence of the fluctuations at fixed T, as well as the T dependence at $n = \text{const}$ (which corresponds to the dependence on r_s and Γ, respectively). The latter was mainly used in the classical region of the phase space. On the other hand, in the strong quantum limit, there is only a weak temperature dependence, so the first method is advantagous. To highlight the peculiarities of quantum melting, in the following, we concentrate on the density dependence of the fluctuations.

Figure 2 shows the n dependence of u_ϕ and u_r, at a fixed temperature $T = 5 \times 10^{-4}$, for the magic clusters $N = 12$ and $N = 19$. The first jump of the fluctuations at comparatively low cricitical densities n_o^* corresponds to quantum OM. At densities $n \ge n_o^*$, the angle between particles from neighboring shells can take arbitrary values. There is a significant difference in the magnitude of the melting densities for the clusters under consideration. As in the classical case, the highest stability (highest value n_o^*) is found for the magic clusters, with the maximum value found for $N = 19$. In particular, we obtained the densities of cold orientational melting by extrapolation of our data to zero temperature. The corresponding values for the density and Brueckner parameter $r_s^{(o)}$ are listed in Table II.

Let us now proceed in Fig. 2 to higher densities. We observe a clear second jump of the fluctuations u_ϕ and u_r, which is related to total melting of the WC. It is instructive to compare the state of the cluster before and after this jump; see middle and right shapshots in Fig. 2, respectively. Evidently, when the density is increased, the peaks of the wave functions broaden in radial (and angular) direction until their width becomes comparable with the intershell spacing. As a result, the probability of intershell transfer of electrons grows rapidly, causing a sudden increase of the radial fluctuations and the onset of radial melting. Our simulations revealed that the jumps of u_ϕ and u_r are clearly visible along the whole WC phase boundary. In the limit of zero temperature, we observe cold radial melting; cf. Table II.

Phase boundary of the mesoscopic Wigner crystal.— The results are summarized in Fig. 3 and Tables I and II for various particle numbers. Consider first the line of radial melting "RM." At low densities, $n < 0.03$, crystallization occurs at critical values of $\Gamma = 1/T_r^*$; see the data in Table I. We found that, for magic (nonmagic) clusters, Γ is above (below) the 2D bulk value, $\Gamma_\infty = 137$; e.g., [7]. This shows that nonmagic clusters are more stable

TABLE II. *Quantum* Wigner crystal: critical density and Brueckner parameter r_s for orientational (o) and radial (r) melting at *zero temperature*. $\tilde{T}_{o,(r)}^{\max}$ is the highest possible melting temperature, $\tilde{T} \equiv nT$. The critical parameters $n_o^*, r_s^{(o)}$ and $\tilde{T}_o^{\max}$ for $N = 11$ and 20 are estimates [16].

N	n_o^*	$r_s^{(o)}$	n_r^*	$r_s^{(r)}$	$\tilde{T}_o^{\max}$	$\tilde{T}_r^{\max}$
10	4.5×10^{-3}	4.9×10^{4}	0.120	69	5.0×10^{-8}	2.2×10^{-4}
11	*5×10^{-3}*	*4×10^{6}*	*0.148*	*45*	*7×10^{-11}*	*9.4×10^{-4}*
12	1.4×10^{-2}	5102	0.123	66	5.0×10^{-6}	2.4×10^{-4}
19	5.0×10^{-2}	400	0.125	64	6.0×10^{-5}	2.5×10^{-4}
20	*1.7×10^{-6}*	*3×10^{11}*	*0.140*	*51*	*3×10^{-18}*	*7.5×10^{-4}*

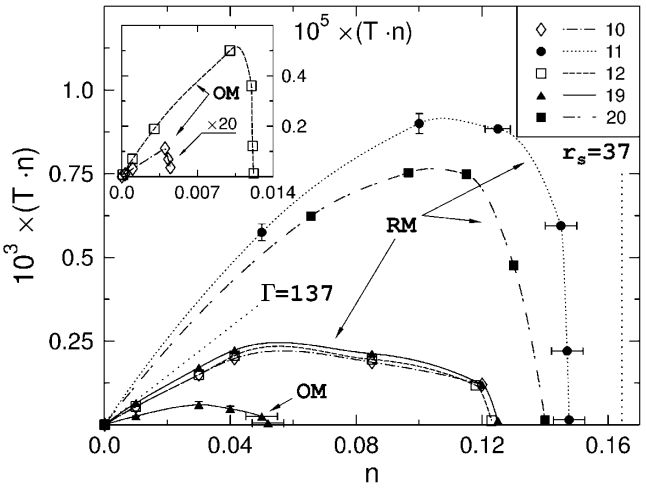

FIG. 3. Phase diagram of the mesoscopic 2D Wigner crystal. "OM" ("RM") denotes the orientational (radial) melting curves for $N = 10$, 11, 12, 19, and 20. Inset shows an enlarged picture of the low-density region. Dotted straight lines indicate the radial melting transition of a macroscopic classical and quantum WC. Brueckner parameter follows from the density by $r_s = 1/n^2$. Error bars shown are typical for all curves.

against radial disordering. The same tendency is observed for cold melting, where the critical values of r_s are systematically lower for nonmagic clusters. Interestingly, for all comparatively small clusters with $10 \leq N \leq 20$, the critical r_s (Table II) exceeds the known value of an infinite 2D system $r_s^\infty \approx 37$ [15]. This systematic deviation from the critical data of a macroscopic system points to the existence of a different scenario of radial melting typical for finite systems. For example, for clusters with $N = 10$ (19), when approaching the phase boundary, we observe increasingly frequent transitions between the shell configurations $\{2, 8\} \leftrightarrows \{3, 7\}$ ($\{1, 6, 12\} \leftrightarrows \{1, 7, 11\}$). The explanation is the lowering of the potential barrier for intershell transitions of individual electrons between these two energetically rather close configurations.

A particularly interesting feature which is missing in infinte systems is the existence of the second transition characterized by freezing of the intershell rotation; cf. areas bounded by the lines "OM" in Fig. 3. This highly ordered state is confined to the region of low density and low temperature. Its phase boundary is highly sensitive to the angular symmetry of the cluster. The most symmetric clusters are the magic ones which are essentially more stable against orientational melting which is seen in their relatively low values of Γ_o^* and $r_s^{(o)}$; cf. Tables I and II. The critical values for the nonmagic clusters are several orders of magnitude larger, confining their orientationally ordered state to much lower densities and temperatures. Finally, the last two columns of Table II contain the maximum temperatures at which the orientationally and radially ordered crystal phases may exist.

In summary, we have presented a detailed PIMC analysis of Wigner crystallization of finite electron systems confined in a 2D harmonic trap including the critical data in the whole density-temperature plane. We have shown that there exist two phases characterized by radial and radial plus angular ordering, respectively, which is essentially different from macroscopic systems. The phase boundaries have been found to be very sensitive to the electron number and to the shell symmetry. In contrast to classical clusters, we observed cold orientational and radial melting which is governed by the spread of the electron wave functions in angular and radial directions. The predictions of our model calculations are expected to be relevant, in particular, for electrons in external fields. Furthermore, they lead us to expect Wigner crystallization also in small 2D islands of electrons (holes) in semiconductor heterostructures: for example, in GaAs/AlGaAs systems, crystallization is predicted for carrier densities below approximately 10^8 cm^{-2} [$(10^9$–$10^{10})$ cm^{-2}] and for temperatures below 1.6–5.5 K, for confinement potentials of 3–10 meV.

This work is supported by the Deutsche Forschungsgemeinschaft (Schwerpunkt "Quantenkohärenz in Halbleitern") and the NIC Jülich.

[1] R. C. Ashoori, Nature (London) **379**, 413 (1996).
[2] C. Yannouleas and U. Landman, Phys. Rev. Lett. **82**, 5325 (1999).
[3] R. Egger *et al.,* Phys. Rev. Lett. **82**, 3320 (1999).
[4] E. Wigner, Phys. Rev. **46**, 1002 (1934).
[5] We use the notations "crystal," "melting," and "phase transitions" to underline the analogy to the corresponding phenomena in infinite systems.
[6] Yu. E. Lozovik, Sov. Phys. Usp. **30**, 912 (1987).
[7] V. M. Bedanov and F. M. Peeters, Phys. Rev. B **49**, 2667 (1994), and references therein.
[8] V. A. Schweigert and F. M. Peeters, Phys. Rev. B **51**, 7700 (1995).
[9] Yu. E. Lozovik and E. A. Rakoch, Phys. Rev. B **57**, 1214 (1998).
[10] For bosonic clusters, see A. I. Belousov and Yu. E. Lozovik, JETP Lett. **68**, 858 (1998).
[11] The WC is very weakly influenced by spin correlations which become important at strong overlap of individual electrons at $r_s < 10$ [3]; cf. Table II.
[12] We found that, in the crystal phase, r_0 is very close (within about 5%) to the mean interparticle distance $\bar{r}$ (first maximum of the pair distribution function).
[13] D. Ceperley, Rev. Mod. Phys. **67**, 279 (1995).
[14] Shown is the distribution of closed electron paths, e.g., [13], averaged over the Monte Carlo chain while keeping the electron positions (the ends of the paths) fixed.
[15] B. Tanatar and D. M. Ceperley, Phys. Rev. B **39**, 5005 (1989).
[16] The relations $n_{o,r}^* \sim \sqrt{T_{o,r}^*}$ and $\tilde{T}_{o,r}^{\max} \sim n_{o,r}^*/(2\Gamma_{o,r}^*)$ are in good qualitative agreement with our data.